



Deposited via The University of Sheffield.

White Rose Research Online URL for this paper:

<https://eprints.whiterose.ac.uk/id/eprint/209406/>

Version: Accepted Version

---

**Article:**

Shao, B., Zhu, Y., Hu, J. et al. (2024) Chemical engineering solution for carbon neutrality in cement industry: Tailor a pathway from inevitable CO<sub>2</sub> emission into syngas. *Chemical Engineering Journal*, 483. 149098. ISSN: 1385-8947

<https://doi.org/10.1016/j.cej.2024.149098>

---

© 2024 The Authors. Except as otherwise noted, this author-accepted version of a journal article published in *Chemical Engineering Journal* is made available via the University of Sheffield Research Publications and Copyright Policy under the terms of the Creative Commons Attribution 4.0 International License (CC-BY 4.0), which permits unrestricted use, distribution and reproduction in any medium, provided the original work is properly cited. To view a copy of this licence, visit <http://creativecommons.org/licenses/by/4.0/>

**Reuse**

This article is distributed under the terms of the Creative Commons Attribution (CC BY) licence. This licence allows you to distribute, remix, tweak, and build upon the work, even commercially, as long as you credit the authors for the original work. More information and the full terms of the licence here:

<https://creativecommons.org/licenses/>

**Takedown**

If you consider content in White Rose Research Online to be in breach of UK law, please notify us by emailing [eprints@whiterose.ac.uk](mailto:eprints@whiterose.ac.uk) including the URL of the record and the reason for the withdrawal request.



20 B. S., Z. X. and Y. Z. performed the process simulations and conducted the analysis. H. L. and Y. Z.  
21 provided constructive suggestions. B. S. wrote the manuscript. J. H., M. W. and F. Q. contributed to  
22 manuscript editing. All authors discussed the results and assisted during manuscript preparation.

## 23 Corresponding authors

24 Correspondence to: Jun Hu, Meihong Wang and Feng Qian

25 \*E-mails: [junhu@ecust.edu.cn](mailto:junhu@ecust.edu.cn), [meihong.wang@sheffield.ac.uk](mailto:meihong.wang@sheffield.ac.uk), [fqian@ecust.edu.cn](mailto:fqian@ecust.edu.cn)

## 26 Abstract

---

27 Cement production is one of the largest industrial sources of CO<sub>2</sub> emissions due to the thermal  
28 decomposition of limestone (CaCO<sub>3</sub>). We combine the chemical engineering strategy into the cement  
29 production and propose a novel process of “Carbonate Dry Reforming of Methane (CaDRM)” that  
30 converts the limestone (CaCO<sub>3</sub>) directly into the cement clinker precursor (CaO) and syngas (CO+H<sub>2</sub>)  
31 through reacting with methane (CH<sub>4</sub>). Thermodynamic analysis indicates the reaction temperature of  
32 CaDRM is lowered by at least 200°C compared with CaCO<sub>3</sub> thermal decomposition. Lab scale  
33 experimental studies show a 95% CaO yield at a 91% syngas selectivity and 90% CH<sub>4</sub> conversion in  
34 CaDRM using cement raw meal at 700°C. Process simulation scale-up and economic analysis indicate  
35 CaDRM pathway can reduce 37.2% CO<sub>2</sub> emission in comparison with the conventional CaCO<sub>3</sub> thermal  
36 decomposition pathway. More significantly, the net profit of \$271.0/t (clinker) can be achieved by the  
37 value-added syngas products and the energy saving. The economic and environmental benefits of the  
38 proposed CaDRM strategy can help its future commercial deployment.

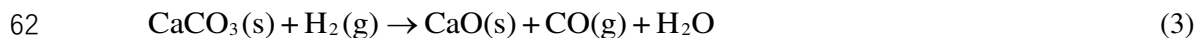
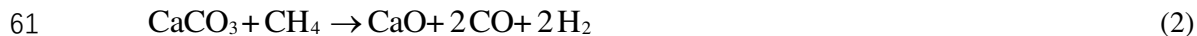
## 39 **Introduction**

---

40 Thermal decomposition of inorganic metal carbonates is one of the most important chemical  
41 processes in industries including cement, steel and non-ferrous metals metallurgy<sup>1-3</sup>. Nevertheless, the  
42 high-temperature decomposition of carbonates is inevitably accompanied by massive CO<sub>2</sub> emissions and  
43 huge energy consumptions. Among them, the cement production (2.8 Gt/y) is currently the largest single  
44 industrial source of carbon emissions, accounting for about 8% of global CO<sub>2</sub> emissions<sup>4</sup>. Analysis along  
45 the carbon footprint of the cement production reveals process-related CO<sub>2</sub> emissions from the  
46 decomposition of limestone (CaCO<sub>3</sub>) (**Eq. 1**) in the pre-calciner account for more than 60% of total  
47 emissions and energy-related CO<sub>2</sub> emissions from the combustion of fossil fuel for maintaining high  
48 temperatures of rotary kiln (1,450°C-1,500°C) and pre-calciner (~900°C) account for the left 40% of total  
49 emissions (**Figure 1a, black pathway**)<sup>5</sup>.

50 To reduce the carbon emissions from the cement industry, many chemical engineering strategies have  
51 been proposed in the cement production, including using the carbonate-free raw materials<sup>6-8</sup>, replacing the  
52 energy supplies with renewable energies<sup>9,10</sup> and implementing carbon capture, utilization and storage  
53 (CCUS) technologies<sup>11,12</sup>. Specifically, when the captured CO<sub>2</sub> is used as a feedstock to produce valuable  
54 fuels and chemicals through various hydrogeneration processes such as Fischer-Tropsch and  
55 methanation<sup>13-16</sup>, it might compensate for some capital investments and operation costs of CO<sub>2</sub> capture.  
56 However, facing the challenges of the huge production but relatively low profits<sup>17,18</sup>, the cement industry  
57 is keenly aware of difficulties to bear high-cost carbonate-free raw materials, renewable energies, and  
58 additional high costs of CCUS technology<sup>19,20</sup>. Therefore, it is of great urgency to develop innovative

59 technologies to achieve the carbon neutrality in cement industry.



63 We propose a novel strategy of direct reduction of carbonate by methane, namely Carbonates Dry  
64 Reforming of Methane (CaDRM) (**Figure 1a, orange pathway**). Different from conventional dry  
65 reforming of methane (DRM) with captured CO<sub>2</sub> from the process-related and energy-related emissions  
66 <sup>21,22</sup>, the proposed CaDRM strategy lies in the methane reforming of the carbonate in one chemical  
67 process without producing any CO<sub>2</sub> but syngas (H<sub>2</sub>+CO) production (**Eq. 2**). One inherent benefit of such  
68 a process is that it allows the simultaneous productions of clinker- precursor (CaO) and valuable syngas.  
69 In addition, the overall energy penalties are expected to be significantly reduced due to the integrated  
70 processes, avoiding the temperature swing between CO<sub>2</sub> capture and utilization, as well as consequent  
71 treatments after the CO<sub>2</sub> capture such as desorption, compression, and transportation. So far, to the best of  
72 our knowledge, there is no report on the direct reduction of carbonates by CH<sub>4</sub>. Fortunately, an  
73 interesting observation reported by Giardini et al. <sup>23</sup> and Reller et al. <sup>24</sup> on the possibility of the  
74 degradation of carbonates in a H<sub>2</sub> atmosphere to form hydrocarbon at comparably low temperatures (**Eq.**  
75 **3**). Baldauf-Sommerbauer et al.<sup>25</sup> illustrated the feasibility of reduction of iron ores (FeCO<sub>3</sub>) with  
76 hydrogen, which can theoretically decrease CO<sub>2</sub> emissions by 60% and reduce agent up to 33% for iron  
77 production. Very recently, Wu's group<sup>26</sup> and Duan's group<sup>27,28</sup> both found the auto-catalytic activity of the  
78 hydrogenation reduction of calcium carbonates for the migration of CO<sub>2</sub> emission into CO and CH<sub>4</sub>

79 productions. Compared with those carbonate hydrogenation, the proposed CaDRM strategy can be a more  
80 efficient way to change CO<sub>2</sub> emissions into syngas production due to the fully atomic utilization  
81 efficiency of CH<sub>4</sub><sup>29-31</sup>. More significantly, in comparing with H<sub>2</sub> source, CH<sub>4</sub> possesses more advantages  
82 such as the abundancy in nature (nature gas), mature industrial applications, and most importantly being  
83 cost-effective<sup>32,33</sup>. Inspired by our previous study of integrated CO<sub>2</sub> capture and conversion which  
84 explicitly identified the synergistic promotion of the carbonate reduction by CH<sub>4</sub> for the regeneration<sup>34</sup>,  
85 we highly anticipate the CaDRM strategy can bring a disruptive technological revolution for achieving  
86 net-zero in the CO<sub>2</sub> emission-intensive cement industry.

87 Herein, combining the thermodynamic analysis and experimental verifications, we firstly  
88 demonstrated the feasibility of CaDRM that the reaction temperature can be lowered by at least 200°C in  
89 comparison with the thermal CaCO<sub>3</sub> decomposition. Furthermore, with the help of Ni/CaO catalyst, not  
90 only the CaCO<sub>3</sub> powder, but also the real cement raw meal can successfully achieve a 95% CaO yield  
91 with at a least 91% syngas selectivity and 90% CH<sub>4</sub> conversion at lower temperature of 700°C. In addition,  
92 to distinguish the carbon mitigation advantages of the CaDRM process, a comparative process of CaCO<sub>3</sub>  
93 thermal decomposition with the CO<sub>2</sub> capture and utilization (CCU) processes of MEA-scrubbing and  
94 DRM was established as well. Economic assessment based on the process simulations further illustrated  
95 the significance of CaDRM by the comparisons of the energy consumption, CO<sub>2</sub> emissions, and operating  
96 costs. As such, the proposed CaDRM process can be a promising strategy to synergistically reduce the  
97 carbon emissions from both sides of the production pathway and energy conservation.

98

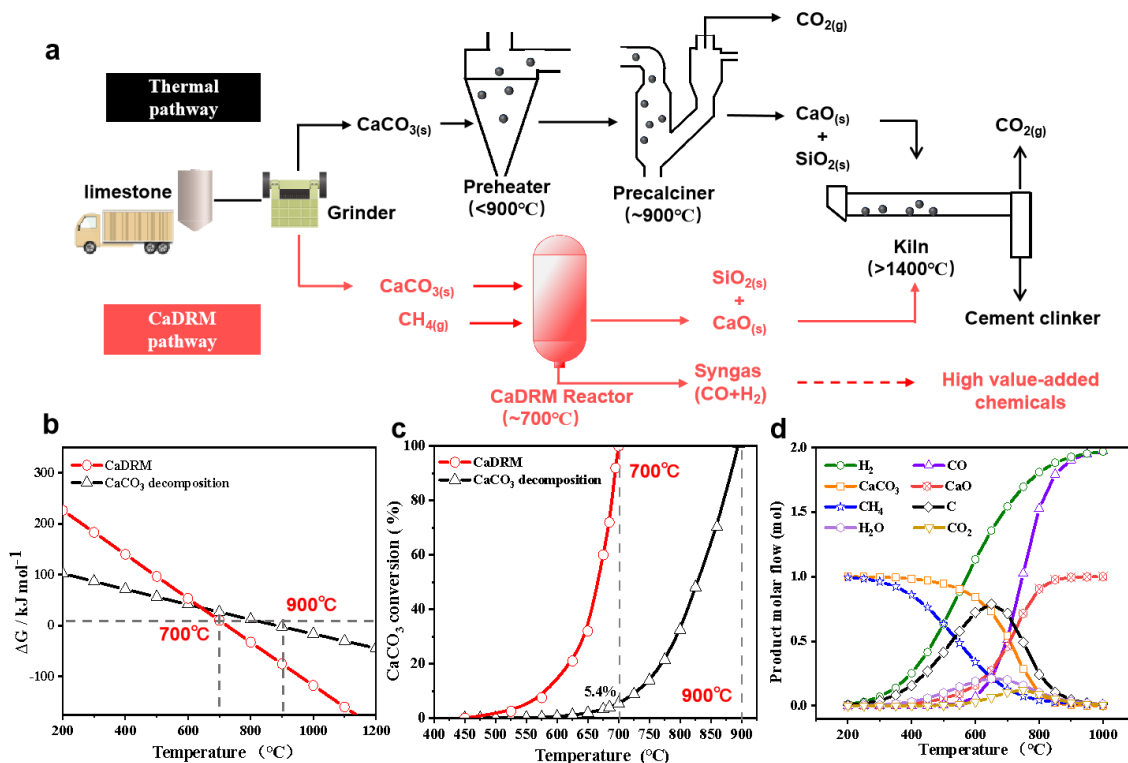
## 99 **Results and discussion**

---

### 100 **Thermodynamic analysis**

101 To evaluate the feasibility of the proposed CaDRM strategy, thermodynamic analysis was firstly  
102 performed by comparing the reductive decomposition of  $\text{CaCO}_3$  in a  $\text{CH}_4$  atmosphere with the  
103 conventional  $\text{CaCO}_3$  thermal decomposition. CaDRM reaction depends much on the temperature and  
104 becomes thermodynamic favorable since its Gibbs free energy is lower than the  $\text{CaCO}_3$  thermal  
105 decomposition above  $630^\circ\text{C}$  (**Figure 1b**). More importantly, the CaDRM reaction starts at as low as  
106  $475^\circ\text{C}$ , and completes at  $700^\circ\text{C}$  (**Figure 1c**), which is about  $200^\circ\text{C}$  lower than the theoretical complete  
107 conversion of the  $\text{CaCO}_3$  thermal decomposition at  $900^\circ\text{C}$ . Whereas at  $700^\circ\text{C}$ , the conversion of  $\text{CaCO}_3$   
108 thermal decomposition is only 5.4%. Therefore, the direct reduction of  $\text{CaCO}_3$  by methane in CaDRM is  
109 thermodynamically feasible, not only lowering down the total energy penalty of  $\text{CaCO}_3$  thermal  
110 decomposition through reducing decarboxylation temperature, but also removing  $\text{CO}_2$  emissions from the  
111 production source<sup>35</sup>.

112 In addition to the direct reduction of  $\text{CaCO}_3$  by  $\text{CH}_4$ , CaDRM is actually a complex system with  
113 multiple side reactions occurring simultaneously, such as the thermal decomposition of  $\text{CaCO}_3$ ,  $\text{CH}_4$   
114 cracking,  $\text{CO}_2$  hydrogenation, reversible water-gas-shift reaction (RWGS) (**Eq. S1-S5, S1**). To predict the  
115 operating temperature windows, we calculated the composition distributions of all possible products  
116 along with the temperature in the complex CaDRM system (**Figure S1**). Below  $650^\circ\text{C}$ , the  $\text{CaCO}_3$   
117 decomposition is unfavorable, whereas the  $\text{CH}_4$  cracking is thermodynamically dominant, giving a  
118 significantly increased  $\text{H}_2$  generation and carbon deposit<sup>36</sup>. When raising the temperature to above  $700^\circ\text{C}$ ,



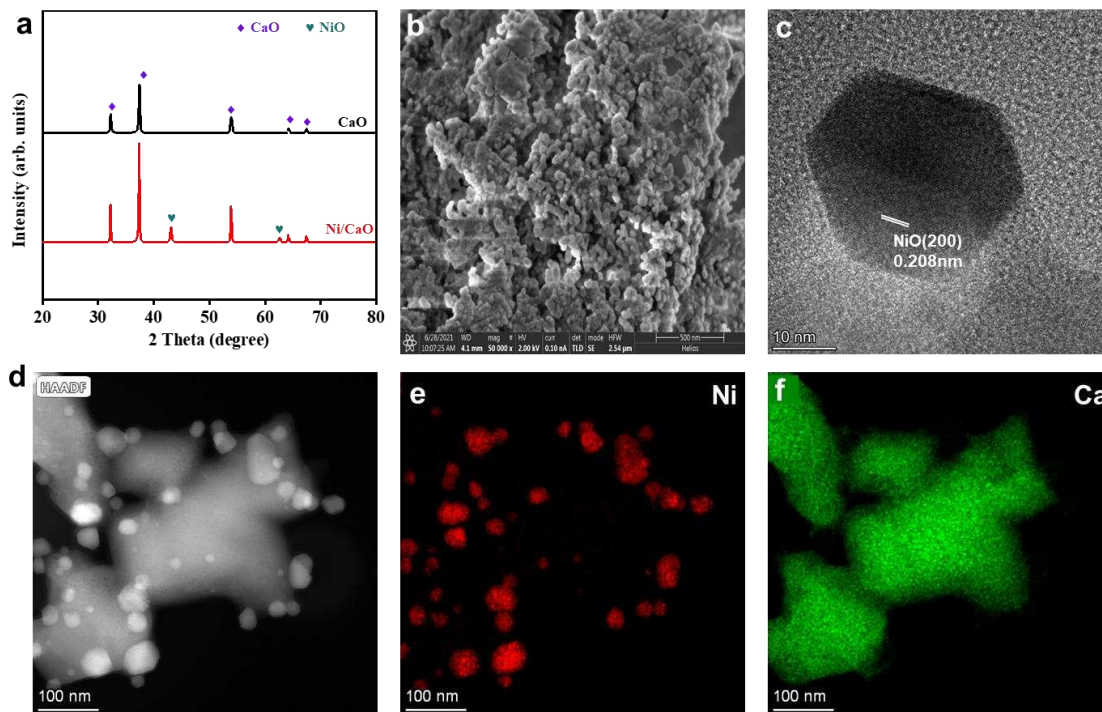
119  
 120 **Figure 1 Comparison of CaDRM pathway with conventional  $\text{CaCO}_3$  thermal decomposition for**  
 121 **cement clinker production.** (a) overview of the incumbent thermal decomposition process (black) and  
 122 the proposed CaDRM process (orange) for manufacturing cement clinker. In the thermal pathway,  
 123 limestone ( $\text{CaCO}_{3(s)}$ ) is heated to above  $900^\circ\text{C}$  in the precalciner for the  $\text{CaCO}_{3(s)}$  decarbonate into  $\text{CaO}_{(g)}$   
 124 and  $\text{CO}_{2(g)}$ . In the CaDRM pathway,  $\text{CaCO}_{3(s)}$  is converted with  $\text{CH}_{4(g)}$  into  $\text{CaO}_{(s)}$  in a CaDRM reactor  
 125 which also generates valuable syngas ( $\text{CO}_{(g)}$  and  $\text{H}_{2(g)}$ ). (b) Gibbs free energy of  $\text{CaCO}_3$  thermal  
 126 decomposition and CaDRM reactions as a function of temperature. (c) The relationship between the  
 127 decomposition conversion rate of  $\text{CaCO}_3$  and temperature. (d) The effect of reaction temperature on the  
 128 distributions of most probable products in CaDRM system with considering the slide reactions at 1 atm  
 129 and  $\text{CH}_4$  to carbonate molar ratios of 1:1.

130  
 131 the transition decline of carbon deposit and rapid increase of  $\text{CO}$  suggest the CaDRM reaction is  
 132 dominant. When the temperature further increases to above  $850^\circ\text{C}$ , the complete decomposition of  
 133  $\text{CaCO}_3$  is achieved and the formation rate of  $\text{H}_2$ ,  $\text{CO}$  and  $\text{CaO}$  reaches the maximum values, respectively.  
 134 Notably, during the whole temperature region, the content of  $\text{CO}_2$  composition is very low. After an initial

135 small increase, it decreases again and completely eliminates when the temperature is up to 800°C.  
136 Therefore, the system of CaDRM is primarily temperature-dependent and high temperature is beneficial  
137 for the CO<sub>2</sub> DRM, RWGS, and CaDRM (**Figure 1d**). Furthermore, increasing the initial molar ratio of  
138 CH<sub>4</sub> to CaCO<sub>3</sub>, the H/C molar ratio in the syngas production can be effectively controlled, but the carbon  
139 deposit inevitably occurs due to the excessive CH<sub>4</sub> cracking (**Figure S1**). This needs to be addressed to  
140 maintain the quality of clinker production.

### 141 **Experimental verifications**

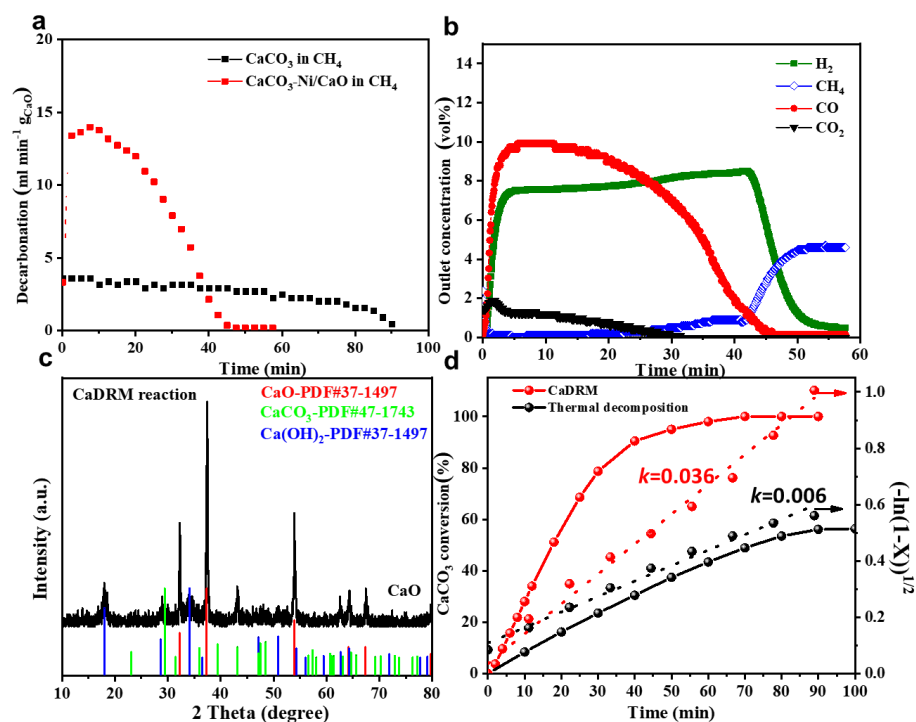
142 To experimentally verify the proposed CaDRM route, we investigated the CaDRM performance in a  
143 fixed-bed column with an inner diameter of 10 mm in the temperature range of 700 - 800°C (**Figure S2**).  
144 A cement compatible catalyst of Ni/CaO was applied to drive the proposed CaDRM process. Prepared by  
145 a simple one-pot sol-gel method, the X-ray diffraction (XRD) pattern (**Figure 2a**) of as-synthesized  
146 Ni/CaO evidence the presence of NiO with its (200) diffraction peak at  $2\theta=43.2^\circ$ . The average crystallite  
147 size was calculated to be 25.6 nm based on the Scherrer equation. The scanning electron microscope  
148 (SEM) image shows Ni/CaO catalyst is composed of the aggregated nanoparticles (**Figure 2b**), with a  
149 Brunauer–Emmett–Teller specific area of 21.0 m<sup>2</sup> g<sup>-1</sup> and a mean pore size of 50 nm (**Figure S3**). The  
150 HAADF-STEM and the energy-dispersive X-ray elemental mapping images reveal that NiO particles are  
151 highly dispersed in the CaO matrix. High-resolution transmission electron microscope (HRTEM) image  
152 further illustrates the high crystallinity of the hexagonal NiO, with clear (200) lattice fringes of 0.208 nm  
153 spacing (**Figure 2c-2f**).



154  
 155 **Figure 2 Structural characterization of catalyst.** (a) XRD pattern of CaO and Ni/CaO. (b) SEM image  
 156 of Ni/CaO. Scale bar, 500 nm. (c) HRTEM of Ni/CaO. Scale bar, 10 nm. (d) STEM image of Ni/CaO. (e-f)  
 157 Energy-dispersive X-ray elemental mapping of Ni/CaO. Scale bar, 100 nm.

158  
 159 As expected, with the help of Ni/CaO catalyst, the degradation of  $\text{CaCO}_3$  starts at lower temperature  
 160 of 700 °C in a  $\text{CH}_4$  atmosphere, the decarbonation shows a sharp triggering and complete in 45 min  
 161 (**Figure 3a and 3b**). After the magnetic separation of the Ni/CaO catalyst (**Figure S4**), the XRD pattern  
 162 of the solid products of catalytic CaDRM shows the characteristic peaks of CaO, containing very weak  
 163 peaks of  $\text{Ca}(\text{OH})_2$  due to the atmospheric humidity (**Figure 3c**). The calculated conversion efficiency of  
 164  $\text{CaCO}_3$  is as high as 95% (**Figures 3d and S5**). Meanwhile, the generation of CO and  $\text{H}_2$  (syngas) can be  
 165 clearly observed after the triggering in the gaseous elution, with the molar ratio of  $\text{H}_2$ : CO:  $\text{CO}_2$  of  
 166 17.2:14.3:1. The produced syngas shows a high selectivity of 96.9% and the reaction rate could be up to  
 167  $0.38 \text{ mmol min}^{-1}$ , which can be further applied to the Fischer-Tropsch reactions for producing high value-

168 added chemicals and fuels. In contrast, without adding any catalysts, a very slow decarbonation occurs as  
 169 the conventional  $\text{CaCO}_3$  thermal decomposition due to the formidable activation energy necessary to  
 170 disrupt the stable C–H bond within the methane molecule. It takes more than 90 min to accomplish the  
 171 surface decomposition at  $700^\circ\text{C}$ . The XRD pattern further indicates the existing of CaO in solid products,  
 172 but a large amount of  $\text{CaCO}_3$  remained (**Figure S6**), and the conversion efficiency of  $\text{CaCO}_3$  is as low as  
 173 50.3% (**Figure 3d**). No CO signal can be observed in the whole detecting temperature range in the  
 174 gaseous elution curve, except for a  $\text{CO}_2$  peak starting at  $780^\circ\text{C}$  and  $\text{H}_2$  at up to  $800^\circ\text{C}$  (**Figure S7**). These  
 175 inconsistent experimental results indicate that although CaDRM reaction is thermochemically favorable,  
 176 the actual process could be kinetically limited without proper catalysts.



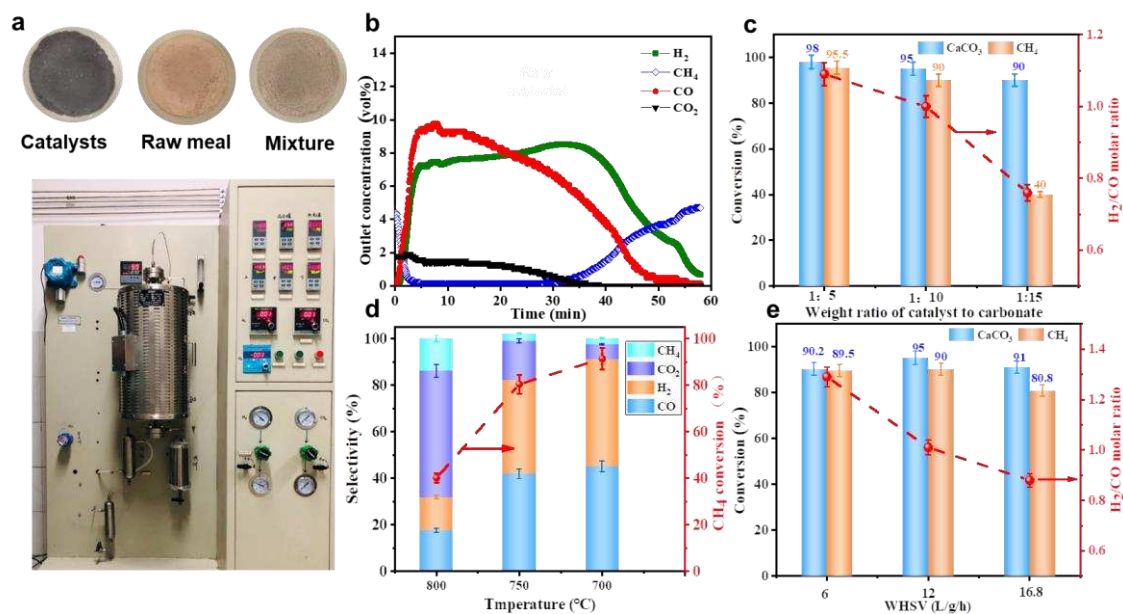
177  
 178 **Figure 3 Comparison of decarbonation kinetics between the CaDRM and the conventional  $\text{CaCO}_3$**   
 179 **thermal decomposition.** (a) Decarbonation rate as a function of time at  $700^\circ\text{C}$ . (b) Molar flow rates of  
 180 CO,  $\text{H}_2$ ,  $\text{CH}_4$  and  $\text{CO}_2$  in the gaseous elution of CaDRM reaction. (c) The XRD patterns of solid products  
 181 of CaO and  $\text{Ca(OH)}_2$  obtained from CaDRM at  $700^\circ\text{C}$ . (d) The conversion rates of  $\text{CaCO}_3$  and its

182 dynamic fitting curves of CaDRM and CaCO<sub>3</sub> thermal decomposition under 700°C.

183 Notably, the shortened reaction time required to accomplish CaDRM is almost a half of that required  
184 for conventional CaCO<sub>3</sub> thermal decomposition at 700°C. The kinetic analysis of the gas-solid  
185 heterogeneous decarbonation of CaCO<sub>3</sub> in different pathways of CaDRM and thermal decomposition  
186 were further illustrated. Fitted well by the modified Avrami-Erofeev (A-V) Equation, respectively ( $R^2 >$   
187 0.9889), the value of the kinetic constant ( $k$ ) of CaDRM route is calculated as high as 0.036, 6-time higher  
188 than the  $k$  of 0.006 of CaCO<sub>3</sub> thermal decomposition at 700°C (**Figure 3d**). This can be attributed to the  
189 effect of Le Chatelier's principle, that the continuous consumption of the CO<sub>2</sub> from CaCO<sub>3</sub> by the CH<sub>4</sub>  
190 reforming on the catalytic sites of Ni can significantly shift the thermodynamic equilibrium of the CaCO<sub>3</sub>  
191 decomposition, providing an additional driving force for fast decarbonation<sup>37</sup>.

192 Inspired by the excellent performance of high conversion efficiencies and superior reaction kinetics  
193 of CaCO<sub>3</sub> at the lower temperature, we validated the CaDRM using real cement raw meals. The average  
194 particle size of raw meal is in the range 50-100  $\mu\text{m}$ , and the compositions are very complex, consisting of  
195 71.43% CaCO<sub>3</sub> and other remains such as Si, Fe, Al by ICP-OES. Excitingly, the molar flow rate of CH<sub>4</sub>,  
196 CO, H<sub>2</sub> and CO<sub>2</sub> in the gaseous elution demonstrate the success of the CaDRM in reality, that a complete  
197 CaCO<sub>3</sub> conversion at a 100% CO selectivity with 90% methane utilization efficiency can be perfectly  
198 achieved at 700°C (**Figure 4a and 4b**). During the CaDRM process, the CaCO<sub>3</sub> concentration decreases  
199 with time, accordingly, the whole process can be divided into three stages. The first very fast stage (0-10  
200 min), the sharply increased flows of H<sub>2</sub> and CO with only a little unconverted CO<sub>2</sub> and CH<sub>4</sub> in the elution  
201 indicate an almost complete conversion of CH<sub>4</sub> with CaCO<sub>3</sub> into syngas. The molar ratio of H<sub>2</sub> to CO is  
202 about 0.9, lower than the predicted thermodynamic equilibrium for the CaDRM at 700°C, suggesting that

203 produced H<sub>2</sub> may also participate in the CaCO<sub>3</sub> hydrogenation<sup>38</sup>. In the second stable stage (10-35 min),  
 204 the decline of CO<sub>2</sub> flow can be ascribed to the depletion of CaCO<sub>3</sub>. While the gradually decreased CO  
 205 flow but the stable H<sub>2</sub> one suggests the water-gas-shift reaction by consuming CO to produce H<sub>2</sub> may  
 206 occur<sup>39</sup>. In the last stage (>35 min), the gradually increased CH<sub>4</sub> flow and the decreased CO flow  
 207 demonstrate the almost complete CaCO<sub>3</sub> conversion. Meanwhile, the simultaneously decreased H<sub>2</sub> flow  
 208 indicates that the CH<sub>4</sub> cracking seldom occurs at 700°C.



209  
 210 **Figure 4 The CaDRM performance of real cement raw meals over Ni/CaO catalyst.** (a) The fixed-  
 211 bed device with the mixture of catalysts and cement raw meal for CaDRM process. (b) Molar flow rates  
 212 of CO, H<sub>2</sub> CH<sub>4</sub> and CO<sub>2</sub> in the gaseous elution during CaDRM reaction. (c) The effect of catalyst ratio on  
 213 calcium carbonate and CH<sub>4</sub> conversion rate. (d) The selectivity of product gas of CaDRM reaction at  
 214 different temperature. (e) Calcium carbonate and CH<sub>4</sub> conversion rate a at different weight hourly space  
 215 velocity (WHSV) of methane. The error bars represent the standard deviation of three independent  
 216 measurements.

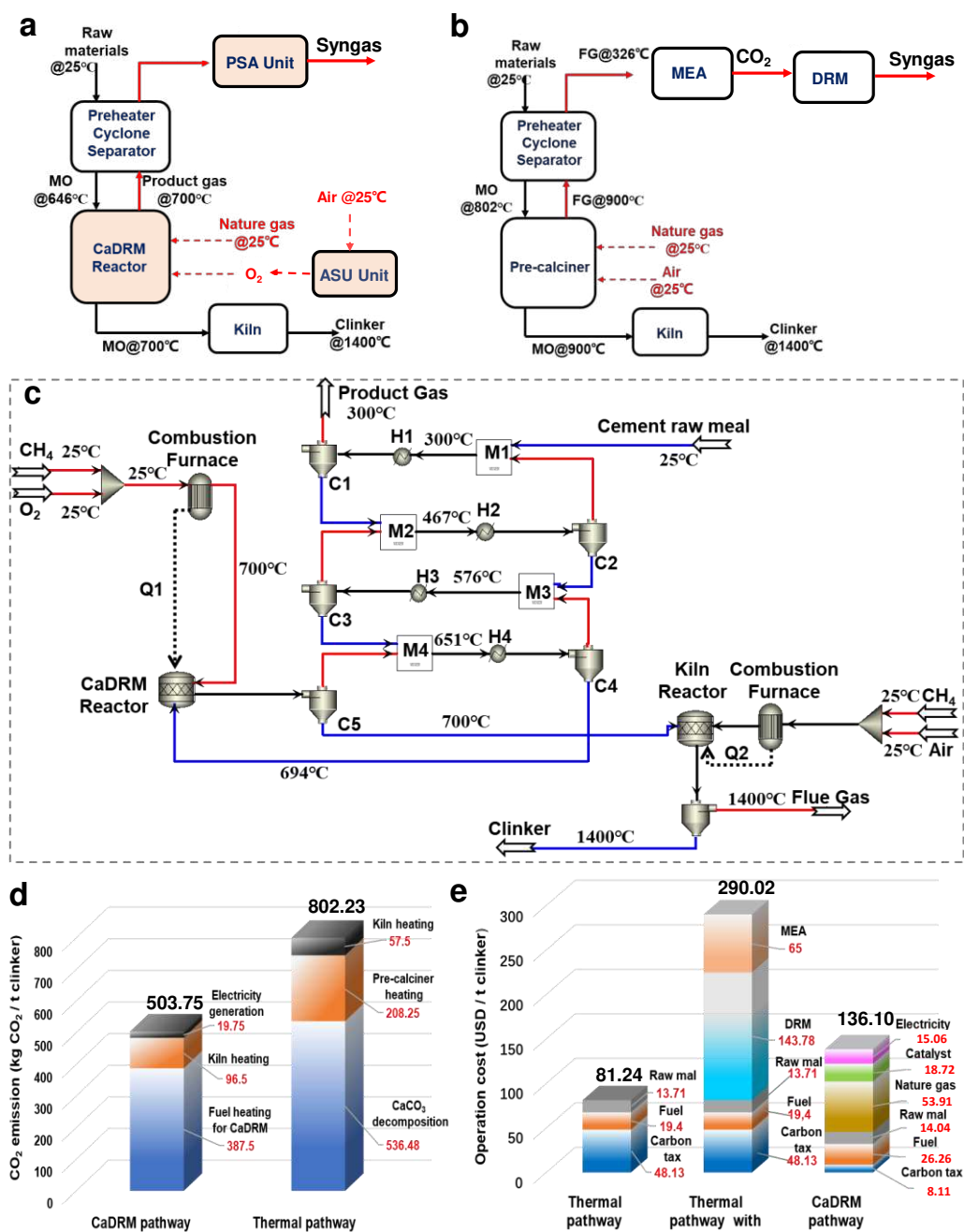
217  
 218 Furthermore, we optimized the operating conditions to enhance the CaDRM performance. By  
 219 optimizing the weight ratio of catalyst to cement raw meal at 1:10, the CaCO<sub>3</sub> and CH<sub>4</sub> conversion

220 efficiency of 95% and 90%, with syngas selectivity of 91.0%, can be achieved, respectively (**Figures 4c**  
221 **and S8a**). In addition, consistent with the thermodynamic predictions, the reaction temperature plays a  
222 pivotal role in selectivity of syngas and conversion of  $\text{CaCO}_3$ . The complete conversion time of cement  
223 raw meals shortens with rising reaction temperature, from 45 min at 700°C to 15 min at 800°C, but the  
224 selectivity of syngas including CO and  $\text{H}_2$  decreases significantly from 91.0% to 31.8% (**Figures 4d** and  
225 **S9**), which can be caused by the competitive thermal decomposition of  $\text{CaCO}_3$ . Moreover, the weight  
226 hourly space velocity (WHSV) of the  $\text{CH}_4$  feed were also investigated. Along with increasing WHSV  
227 from  $6 \text{ L g}^{-1} \text{ h}^{-1}$  to  $16.8 \text{ L g}^{-1} \text{ h}^{-1}$ , methane and carbonate conversion rate increases first to a maximum and  
228 then decreases, however, the selectivity of syngas decreases from 93.9% to 82.2% which can be attributed  
229 to the lower methane conversion (**Figures 4e** and **S8b**). Moreover, the higher WHSV means the  
230 shortened residence time of gas-solid reaction, so the methane conversion and the molar ratio of  $\text{H}_2/\text{CO}$   
231 decrease at higher WHSV. Therefore, a suitable WHSV of  $\text{CH}_4$  is  $12 \text{ L g}^{-1} \text{ h}^{-1}$  for a high selectivity of  
232 syngas and regulating the  $\text{H}_2/\text{CO}$  ratio of 1.0 (**Table S1**). Notably, the XRD patterns of the cement raw  
233 meal and the obtained solid products of dominated CaO further confirm the validity of CaDRM (**Figure**  
234 **S10**), which can subsequently produce the clinker precursor in the kiln. As such, CaDRM will be a  
235 promising strategy for future large scale cement production with low carbon emission and low energy  
236 consumption.

### 237 **Process Simulation and Preliminary Economic Evaluation**

238 To demonstrate the practical feasibility of CaDRM at large scale, we carried out the process  
239 simulation. As CaDRM is the integration of both remarkably endothermic  $\text{CaCO}_3$  thermal decomposition

240 and the DRM reaction, it requires close attention to the heat supply. In this context, we integrated the  
241 process of oxygen enriched combustion of CH<sub>4</sub> with the CaDRM process, namely auto-thermal CaDRM,  
242 since CH<sub>4</sub> acts as both reactant and fuel for the energy supply. By using the Aspen Plus V10<sup>®</sup>, the model  
243 of the clinker production system based on the auto-thermal CaDRM route was constructed, which was  
244 composed of the air separator unit (ASU), heat exchange cyclones, CH<sub>4</sub> combustion furnace, CaDRM  
245 reactor, rotary kiln and pressure swing adsorption unit (PSA) for purification of syngas, respectively  
246 (**Figure 5a**). For the sake of comparison, the referenced clinker production system based on the  
247 conventional CaCO<sub>3</sub> thermal decomposition route was also constructed by combining the additional CO<sub>2</sub>  
248 capture and utilization (CCU) unit. In comparison with CaDRM route, the CCU unit is composed of the  
249 monoethanolamine (MEA) scrubbing for CO<sub>2</sub> capture, which is currently employed in conventional  
250 cement industry and following the DRM reaction for the CO<sub>2</sub> utilization<sup>40,41</sup>. (**Figures 5b and S11**). To  
251 simulate the typical medium sized cement production line with the clinker production capacity of 2500 t/d  
252 (**Tables S2 and S3**), we set the decomposition rate of carbonate in cement raw meal as 95%, and the CH<sub>4</sub>  
253 conversion efficiency as 90%, respectively. The accuracy of the model was first verified by using the  
254 same compositions and feed rate of cement raw meal in the reported conventional clinker-production  
255 system based on the CaCO<sub>3</sub> thermal decomposition route (**Tables S4 and S5**)<sup>42</sup>.



256  
 257 **Figure 5. Process layouts and economic analysis of clinker and syngas co-productions through**  
 258 **CaDRM route instead of the conventional CaCO<sub>3</sub> thermal decomposition.** (a) the auto-thermal  
 259 CaDRM system with ASU and PSA units. (b) the conventional CaCO<sub>3</sub> thermal decomposition system  
 260 with CCU units. (c) Process model of the CaDRM system in Aspen Plus®. (d) CO<sub>2</sub> emissions analysis and  
 261 comparison between two routes of the CaDRM and the conventional thermal decomposition. (e)  
 262 Operating costs of the thermal decomposition pathway with/without CCU and CaDRM pathway.

263 The total energy consumption of the constructed clinker production systems includes three parts: 1)  
 264 the heating supplies for the CaDRM reaction or CaCO<sub>3</sub> thermal decomposition; 2) the heating supplies for  
 265 the high-temperature conversion of metal oxides to clinker in kilns; 3) the energy (electricity) supplies for  
 266 ASU and PSA units in the CaDRM route, or for the CO<sub>2</sub> capture and conversion in the CaCO<sub>3</sub> thermal  
 267 decomposition route. The CO<sub>2</sub> emissions of two systems were converted based on carbon intensity of  
 268 electricity and the total fuels used for the energy supplies. We also estimated the operating costs based on  
 269 the cost of the raw meal, CH<sub>4</sub> as the reactant and fuels, catalysts, electricity, and carbon tax of US \$60 per  
 270 ton CO<sub>2</sub> (Details can be found in SI). To simplify, we did not consider the heat recovery from the kiln and  
 271 the heat loss of flue gas from the CaDRM reactor or the pre-calciner in both cases.

272 **Table 1** Economic assessment of clinker and syngas productions through the CaDRM route.

Operating cost (thousand \$ per day)		Income (thousand \$ per day)	
Raw meal	35.10	Clinker	137.50
catalyst	46.80	Syngas	880.25
Electricity	37.64		
Nature gas	200.43		
CO <sub>2</sub> tax	20.29		
Total	340.26	Total	1017.75
Operating cost	\$136.10/t (clinker)	Average income	\$407.10/t (clinker)
Net income		\$271.00/t (clinker)	

273 <sup>a</sup> Total CO<sub>2</sub> tax on heating for CaDRM reactor and calciner by burning natural gas.

274

275 On the premise of ensuring consistent feeds of the raw meal and output of clinker products, the  
 276 balance of materials and energies of each system were calculated, respectively. (**Figures 5c** and **S12**,

277 **Tables S6 and S7**). Based on these, the economic analysis of two systems were evaluated by comparing  
278 the CO<sub>2</sub> emissions, energy supplies, and operating costs. The proposed system of CaDRM route can  
279 significantly reduce the inevitable carbon emissions of 536.48 kg (CO<sub>2</sub>)/t (clinker) into the syngas by  
280 replacing the thermal decomposition of CaCO<sub>3</sub> with the reduction in a CH<sub>4</sub> atmosphere. Although the  
281 CaDRM process successfully decreases the operating temperature by 200°C, the strongly endothermic  
282 CaDRM reaction plus the consequent high temperature sintering in kilns (1450°C) need additional heat  
283 supplies, resulting in increases of CO<sub>2</sub> emissions by 218.25 kg (CO<sub>2</sub>)/t (clinker). Moreover, to purify the  
284 syngas, the CO<sub>2</sub> emission related to electricity of ASU and PSA unit accounts for 19.75 kg(CO<sub>2</sub>)/t  
285 (clinker). Thus, the CO<sub>2</sub> emissions of the CaDRM system can be significantly reduced by 37.2%, from  
286 802.23 kg (CO<sub>2</sub>)/t (clinker) of the conventional CaCO<sub>3</sub> thermal decomposition to 503.75 kg (CO<sub>2</sub>)/t  
287 (clinker) in overall (**Figure 5d**). Meanwhile, the total energy supplies for the CaDRM system, including  
288 the units of ASU, oxy-combustion, CaDRM reactor, and PSA, are calculated as high as 6.54 GJ/t (clinker).  
289 Although this value is higher than the sole value of the conventional CaCO<sub>3</sub> thermal decomposition of  
290 2.38 GJ/t (clinker), when considering the syngas production for the same evaluation level, the coupled  
291 CO<sub>2</sub> capture and conversion units of 10.46 GJ/t (clinker) and the heat loss caused by the temperature  
292 swing between MEA scrubbing and DRM (**Figure S13, TableS8 and S9**) makes the constructed thermal  
293 decomposition system ultra-high energy consumptions. The significant achievement of a 37.5% reduction  
294 of overall energy consumption in the CaDRM system come from not only the lower operating  
295 temperature, but also avoiding the unreasonable temperature swing between cooling down the flue gas for  
296 the CO<sub>2</sub> capture by MEA-scrubbing and raising up again for the CO<sub>2</sub> conversion by DRM reaction.

297 Accordingly, the economic evaluation based on the 2500 t/d (clinker) production shows that the  
298 operating cost of the CaDRM system is \$340.26k/d, composed of the raw meal (\$35.10k), nature gas feed  
299 (\$200.43k), catalysts attrition (\$46.80k), electricity for ASU and PSA unit (\$37.64k) (**Table 1**). Among  
300 them, the price of nature gas (NG) is the cost-dominant factor for the operating cost of CaDRM process  
301 (**Figure S14**). On the other hand, with the incomes of \$1017.75k/d returned from the 2500 t/d clinker and  
302 1956 t/d syngas products, the revenue of CaDRM process will be about \$407.10/t (clinker), perfectly able  
303 to offset the operating cost of \$136.10/t (clinker), and achieve a net profit of \$271.0/t (clinker) (**Table 1**).  
304 More importantly, the product of syngas with the molar ratio of H<sub>2</sub> to CO of 1 can be further utilized  
305 downstream for higher value-added chemicals and fuels<sup>43,44</sup>. On the contrary, although the operating cost  
306 of the pristine CaCO<sub>3</sub> thermal decomposition is as low as \$81.24/t (clinker), the operating costs of CCU  
307 of the MEA scrubbing and the DRM to produce syngas were calculated as high as \$65.0/t (CO<sub>2</sub>) and  
308 \$143.78/t (CO<sub>2</sub>), respectively (**Figure 5e**). Based on the average CO<sub>2</sub> emission of 0.745 t/t (clinker), the  
309 overall operating cost of the CaCO<sub>3</sub> thermal decomposition with CCUS route is calculated to be at least  
310 \$290.02/t (clinker), which is 113.09% higher than the proposed CaDRM route for clinker and syngas  
311 productions, letting alone the additional operating costs of CO<sub>2</sub> compression and transportation for the  
312 separated CCU processes in general.

## 313 **Conclusion**

---

314 In this study, a novel pathway of “Carbonate Dry Reforming of Methane (CaDRM)” strategy was  
315 proposed and successfully through converting the raw meal (CaCO<sub>3</sub>) directly into the cement clinker  
316 precursor (CaO) and syngas by CH<sub>4</sub>. Thanks to the cement compatible catalyst of Ni/CaO, the CaDRM

317 reaction achieves a complete conversion of  $\text{CaCO}_3$  at a 90% conversion efficiency of  $\text{CH}_4$  at relatively  
318 lower temperature of  $700^\circ\text{C}$ . More significantly, the feasibility of CaDRM was further demonstrated by  
319 adopting the cement raw meal, with the excellent conversion efficiency of 95% for the main component  
320 of  $\text{CaCO}_3$ , 90% for  $\text{CH}_4$ , and selectivity of 91% for syngas, respectively. Based on the process simulations,  
321 the proposed CaDRM system enabled a 37.2% reduction of the  $\text{CO}_2$  emissions and a 37.5% reduction in  
322 overall energy consumption in comparison with the conventional  $\text{CaCO}_3$  thermal decomposition system  
323 with CCU. Economic analysis reveals that the operating costs of this novel CaDRM stands at \$136.10/t  
324 (clinker), 113.09% lower than that of the conventional clinker manufacturing integrated with CCU  
325 processes of MEA-scrubbing and DRM-conversion. Notably, CaDRM process for co-production clinker  
326 and syngas can achieve revenue of \$407.10/t (clinker), with a net profit of \$271.0/t (clinker). Accordingly,  
327 this newly proposed CaDRM technology will reduce  $\text{CO}_2$  emissions and improve the economics at the  
328 same time.

## 329 **Acknowledgements**

---

330 We acknowledge the financial support from the National Natural Science Foundation of China (22278126,  
331 22250005), Intergovernmental International Science and Technology Innovation Cooperation Key Project  
332 (2021YFE0112800) and the Fundamental Research Funds for the Central Universities (2022ZFH04).  
333 The UK author would like to thank the financial support of the EU RISE project OPTIMAL (Grant  
334 Agreement No: 101007963).

335

336

## 337 **Data Availability**

---

338 The data that support the findings of this study are available within the article and supplementary  
339 information or from the corresponding authors on reasonable request. Source data are provided with this  
340 paper.

## 341 **Competing interests**

---

342 The authors declare no competing interests.

## 343 **References**

---

- 344 1. Tian, S., Jiang, J., Zhang, Z. & Manovic, V. Inherent potential of steelmaking to contribute to  
345 decarbonisation targets via industrial carbon capture and storage. *Nat. Commun.* **9**, 4422 -4429  
346 (2018).
- 347 2. Wu, T., Ng, S.T. & Chen, J. Deciphering the CO<sub>2</sub> emissions and emission intensity of cement  
348 sector in China through decomposition analysis. *J. Clean. Prod.* **352**, 131627-131641 (2022).
- 349 3. Yang, Y., et al. Mapping global carbon footprint in China. *Nat. Commun.* **11**, 2237-2244 (2020).
- 350 4. Fennell, P.S., Davis, S.J. & Mohammed, A. Decarbonizing cement production. *Joule* **5**, 1305-  
351 1311 (2021).
- 352 5. Mowbray, B.A.W., Zhang, Z.B., Parkyn, C.T.E. & Berlinguette, C.P. Electrochemical cement  
353 clinker precursor production at low voltages. *ACS Energy Lett.* **8**, 1772-1778 (2023).
- 354 6. Santos, T.A., Cilla, M.S. & Ribeiro, e.D.V. Use of asbestos cement tile waste (ACW) as  
355 mineralizer in the production of Portland cement with low CO<sub>2</sub> emission and lower energy  
356 consumption. *J. Clean. Prod.* **335**, 130061-130072 (2022).
- 357 7. Shah, I.H., Miller, S.A., Jiang, D. & Myers, R.J. Cement substitution with secondary materials  
358 can reduce annual global CO<sub>2</sub> emissions by up to 1.3 gigatons. *Nat. Commun.* **13**, 5758 (2022).
- 359 8. Watari, T., Cao, Z., Hata, S. & Nansai, K. Efficient use of cement and concrete to reduce reliance  
360 on supply-side technologies for net-zero emissions. *Nat. Commun.* **13**, 4158 (2022).
- 361 9. Wojtacha-Rychter, K., Kucharski, P. & Smolinski, A. Conventional and alternative sources of  
362 thermal energy in the production of cement—An impact on CO<sub>2</sub> emission. *Energies* **14**, 1539  
363 (2021).

- 364 10. Rumayor, M., Fernández-González, J., Domínguez-Ramos, A. & Irabien, A. Deep  
365 decarbonization of the cement sector: A prospective environmental assessment of CO<sub>2</sub> recycling  
366 to methanol. *ACS Sustain. Chem. Eng.* **10**, 267-278 (2022).
- 367 11. Benhelal, E., Shamsaei, E. & Rashid, M.I. Novel modifications in a conventional clinker making  
368 process for sustainable cement production. *J. Clean. Prod.* **221**, 389-397 (2019).
- 369 12. Erans, M., et al. Pilot testing of enhanced sorbents for calcium looping with cement production.  
370 *Appl. Energy* **225**, 392-401 (2018).
- 371 13. Sun, J., et al. MOF-Derived Ru<sub>1</sub>Zr<sub>1</sub>/Co dual-atomic-site catalyst with promoted performance for  
372 Fischer–Tropsch synthesis. *J. Am. Chem. Soc.* **145**, 7113-7122 (2023).
- 373 14. Centi, G. & Perathoner, S. The chemical engineering aspects of CO<sub>2</sub> capture, combined with its  
374 utilisation. *Curr. Opin. Chem. Eng.* **39**, 100879 (2023).
- 375 15. Otto, A., Grube, T., Schiebahn, S. & Stolten, D. Closing the loop: captured CO<sub>2</sub> as a feedstock in  
376 the chemical industry. *Energy Environ.Sci.* **8**, 3283-3297 (2015).
- 377 16. Yang, C., et al. Intrinsic mechanism for carbon dioxide methanation over Ru-based nanocatalysts.  
378 *ACS Catal.* **13**, 11556-11565 (2023).
- 379 17. Zhang, Z., et al. Cement clinker precursor production in an electrolyser. *Energy Environ. Sci.*  
380 **15**,5129-5136 (2022).
- 381 18. Zhang, C.-Y., Yu, B., Chen, J.-M. & Wei, Y.-M. Green transition pathways for cement industry in  
382 China. *Resour. Conserv. Recy.* **166**, 105355 (2021).
- 383 19. Chen, X., Matar, M.G., Beatty, D.N. & Srubar, W.V., III. Retardation of Portland cement  
384 hydration with photosynthetic algal biomass. *ACS Sustain. Chem. Eng.* **9**, 13726-13734 (2021).
- 385 20. Benhelal, E., Shamsaei, E. & Rashid, M.I. Challenges against CO<sub>2</sub> abatement strategies in cement  
386 industry: A review. *J. Environ. Sci.* **104**, 84-101 (2021).
- 387 21. Zhu, Q., et al. Enhanced CO<sub>2</sub> utilization in dry reforming of methane achieved through nickel-  
388 mediated hydrogen spillover in zeolite crystals. *Nat. Catal.* **5**, 1030-1037 (2022).
- 389 22. Chen, L., et al. Ternary NiMo-Bi liquid alloy catalyst for efficient hydrogen production from  
390 methane pyrolysis. *Science* **381**, 857-861 (2023).
- 391 23. Giardini A., Salotti C. & Lakner J. Synthesis of graphite and hydrocarbons by reaction between  
392 calcite and hydrogen. *Science* **159**, 317-319(1968).
- 393 24. Reller, A., Padeste, C. & Hug, P. Formation of organic carbon compounds from metal carbonates.  
394 *Nature* **329**, 527-529 (1987).
- 395 25. Baldauf-Sommerbauer, G., Lux, S. & Siebenhofer, M. Sustainable iron production from mineral  
396 iron carbonate and hydrogen. *Green Chem.* **18**, 6255-6265 (2016).

- 397 26. Sun, S., et al. Integrated CO<sub>2</sub> capture and utilization with CaO-alone for high purity syngas  
398 production. *Carbon Capture Sci. Technol.* **1**, 100001 (2021).
- 399 27. Xue, Z., et al. Co-thermal in-situ reduction of inorganic carbonates to reduce carbon-dioxide  
400 emission. *Sci. China Chem.* **66**, 1201-1210 (2023).
- 401 28. Shi, S., et al. Hydrogenation of calcium carbonate to carbon monoxide and methane. *Fuel* **354**,  
402 129385 (2023).
- 403 29. Zhu, Q., et al. Enhanced CO<sub>2</sub> utilization in dry reforming of methane achieved through nickel-  
404 mediated hydrogen spillover in zeolite crystals. *Nat. Catal.* **5**, 1030-1037 (2022).
- 405 30. Zhang, Q., Akri, M., Yang, Y. & Qiao, B. Atomically dispersed metals as potential coke-resistant  
406 catalysts for dry reforming of methane. *Cell Rep. Phys. Sci.* **4**, 101291-101304 (2023).
- 407 31. Wang, J., et al. Investigation of atom-level reaction kinetics of carbon-resistant bimetallic NiCo-  
408 reforming catalysts: Combining microkinetic modeling and density functional theory. *ACS Catal.*  
409 **12**, 4382-4393 (2022).
- 410 32. Galdeano, C., Cook, M. A. & Webber, M. E. Multilayer geospatial analysis of water availability  
411 for shale resources development in Mexico. *Environ. Res. Lett.* **12**, 084014 (2017).
- 412 33. Yu, Y. Mechanisms for the accumulation of deep gas in the southern Songliao Basin. *China. J. Pet.*  
413 *Sci. Eng.* **182**, 106302 (2019).
- 414 34. Shao, B., et al. Synergistic promotions between CO<sub>2</sub> capture and in-situ conversion on Ni-CaO  
415 composite catalyst. *Nat. Commun.* **14**, 996 (2023).
- 416 35. Steinfeld, A. Solar combined thermochemical processes for CO<sub>2</sub> mitigation in the iron, cement,  
417 and syngas industries. *Energy* **19**, 1077-1081 (1994).
- 418 36. Upham, D.C., et al. Catalytic molten metals for the direct conversion of methane to hydrogen and  
419 separable carbon. *Science* **358**, 917-921 (2017).
- 420 37. Tian, S., Yan, F., Zhang, Z. & Jiang, J. Calcium-looping reforming of methane realizes in situ CO<sub>2</sub>  
421 utilization with improved energy efficiency. *Sci. Adv.* **5**, eaav5077 (2019).
- 422 38. Kim, S.M., et al. Integrated CO<sub>2</sub> capture and conversion as an efficient process for fuels from  
423 greenhouse gases. *ACS Catal.* **8**, 2815-2823 (2018).
- 424 39. Liu, H.-X., et al. Partially sintered copper–ceria as excellent catalyst for the high-temperature  
425 reverse water gas shift reaction. *Nat. Commun.* **13**, 867 (2022).
- 426 40. Rezaei, E. & Dzuryk, S. Techno-economic comparison of reverse water gas shift reaction to  
427 steam and dry methane reforming reactions for syngas production. *Chem. Eng. Res. Des.* **144**,  
428 354-369 (2019).
- 429 41. Monteiro, J. & Roussanaly, S. CCUS scenarios for the cement industry: Is CO<sub>2</sub> utilization feasible?

- 430 J. CO<sub>2</sub> Utiliz. **61**, 102015 (2022).
- 431 42. Nhuchhen, D.R., Sit, S.P. & Layzell, D.B. Alternative fuels co-fired with natural gas in the pre-  
432 calciner of a cement plant: Energy and material flows. Fuel **295**, 120544(2021).
- 433 43. Pan, X., Jiao, F., Miao, D. & Bao, X. Oxide–zeolite-based composite catalyst concept that enables  
434 syngas chemistry beyond Fischer–Tropsch synthesis. Chem. Rev. **121**, 6588-6609 (2021).
- 435 44. Wang, C., et al. Direct conversion of syngas to ethanol within zeolite crystals. Chem. **6**, 646-657  
436 (2020).